

Relationships between Beta-Amyloid and Functional Connectivity in Different Components of the Default Mode Network in Aging

Elizabeth C. Mormino¹, Andre Smiljic¹, Amynta O. Hayenga¹, Susan H. Onami¹, Michael D. Greicius², Gil D. Rabinovici^{1,3,4,5}, Mustafa Janabi³, Suzanne L. Baker³, Irene V. Yen³, Cindee M. Madison¹, Bruce L. Miller^{4,5} and William J. Jagust^{1,3,4,5}

¹Helen Wills Neuroscience Institute, University of California Berkeley, Berkeley, CA 94720, USA, ²Department of Neurology and Neurological Sciences, Stanford University School of Medicine, Stanford, CA 94304 USA, ³Division of Life Sciences, Lawrence Berkeley National Laboratory, Berkeley, CA 94720 USA, ⁴Memory and Aging Center, University of California San Francisco, San Francisco, CA 94117, USA and ⁵Department of Neurology, University of California San Francisco, San Francisco, CA 94117 USA

Address correspondence to Elizabeth C. Mormino, Helen Wills Neuroscience Institute, University of California, Berkeley, 132 Barker Hall, MC #3190, Berkeley, CA 94720, USA. Email: bmormino@berkeley.edu.

Although beta-amyloid (A β) deposition is a characteristic feature of Alzheimer's disease (AD), this pathology is commonly found in elderly normal controls (NC). The pattern of A β deposition as detected with Pittsburgh compound-B positron emission tomography (PIB-PET) imaging shows substantial spatial overlap with the default mode network (DMN), a group of brain regions that typically deactivates during externally driven cognitive tasks. In this study, we show that DMN functional connectivity (FC) during rest is altered with increasing levels of PIB uptake in NC. Specifically, FC decreases were identified in regions implicated in episodic memory (EM) processing (posteromedial cortex, ventral medial prefrontal cortex, and angular gyrus), whereas connectivity increases were detected in dorsal and anterior medial prefrontal and lateral temporal cortices. This pattern of decreases is consistent with previous studies that suggest heightened vulnerability of EM-related brain regions in AD, whereas the observed increases in FC may reflect a compensatory response.

Keywords: aging, beta-amyloid, PIB-PET, resting state fMRI

Introduction

Although fibrillar beta-amyloid (A β) plaques are a hallmark of Alzheimer's disease (AD) (Walsh and Selkoe 2007), this pathology is frequently found in cognitively intact older people (Tomlinson et al. 1968; Hulette et al. 1998; Davis et al. 1999; Price and Morris 1999; Knopman et al. 2003; Bennett et al. 2006; Savva et al. 2009). The recent advent of Pittsburgh compound-B positron emission tomography (PIB-PET) imaging allows in vivo investigation of fibrillar A β plaques (Klunk et al. 2004) and has been used to study the relevance of A β deposition in normal controls (NC) (Pike et al. 2007; Jack et al. 2008; Dickerson et al. 2009; Mormino et al. 2009; Rabinovici and Jagust 2009; Sperling et al. 2009; Storandt et al. 2009; Bourgeat et al. 2010). Many researchers speculate that A β accumulation may be an initiating event that leads to neuronal dysfunction and neurodegeneration, cognitive loss, and eventually AD (Walsh and Selkoe 2007; Morris et al. 2009; Jack et al. 2010).

Interestingly, A β plaque deposition shows a high degree of spatial overlap with a network of brain regions that together constitute the default mode network (DMN) (Buckner et al. 2005). Comprised of medial prefrontal, posteromedial (precuneus, posterior cingulate, and retrosplenial), and lateral parietotemporal cortices, as well as the medial temporal lobe, the DMN is typically deactivated during externally driven cognitive tasks and activated during internally driven processes,

such as mind wandering, future planning, and autobiographical memory (Buckner et al. 2008).

The DMN network is commonly studied with task-free resting state functional magnetic resonance imaging (fMRI) (Greicius et al. 2003; Fox et al. 2005). Functional connectivity (FC) analyses of resting state fMRI data capture brain regions showing correlated low frequency (<0.1 Hz) spontaneous activity and have been used to define multiple networks with known anatomical connectivity and coactivation during task-related fMRI (Fox and Raichle 2007). Independent components analysis (ICA) has been employed in some FC studies, robustly defining the DMN, as well as motor, sensory, and frontal-executive networks (Beckmann and Smith 2004; Damoiseaux et al. 2006). Although the biological mechanism underlying these low frequency fluctuations remains unclear, it is possible that resting state networks reflect spontaneous cognitive processes, an intrinsic property of the brain's "baseline" state or a combination of both (Buckner and Vincent 2007; Raichle and Snyder 2007).

Two recent studies combining PIB-PET imaging with resting state fMRI in NC showed that elevated A β deposition measured globally in cerebral cortex was associated with decreases in DMN FC (Hedden et al. 2009; Sheline et al. 2010). A question left unaddressed in these studies is whether the specific pattern of A β deposition is related to dysfunction in specific nodes of the network. Interestingly, there are discrepancies between the location of A β deposition and patterns of neuronal dysfunction seen with both imaging and neuropathology (Arnold et al. 1991; Jack et al. 2008; Bourgeat et al. 2010). In particular, the medial temporal lobe shows pronounced atrophy in AD when it shows little A β deposition, whereas the prefrontal cortex is relatively preserved despite extensive early PIB uptake (Jack et al. 2008). An area of convergence is in the precuneus/posterior cingulate, which shows both early hypometabolism (Minoshima et al. 1997) and A β deposition (Mintun et al. 2006). Studying the DMN in this context is important since nodes of this network reflect both congruence and incongruence in the relationship between A β deposition and neuronal integrity.

The goal of this study was therefore to investigate associations between amyloid deposition and connectivity within the DMN and to examine mechanisms that might underlie network alterations.

Materials and Methods

Subject Recruitment

Older NC subjects were recruited from the community via newspaper advertisement. Eligibility requirements for recruitment in this study

were no MRI contradictions, living independently in the community, Mini-Mental State Examination (MMSE) ≥ 26 , absence of neurological or psychiatric illness, lack of major medical illnesses and medications that affect cognition, and normal performance on cognitive tests. Forty-four subjects underwent PET imaging and fMRI for this study.

Additionally, resting state fMRI data were collected on 17 young subjects to define a template for the DMN (mean age = 23.0 (2.9), 9 females). Young subjects were recruited from the community through online postings. PIB-PET data from 22 AD patients were used for comparison purposes (mean age = 65.9 (10.7), 10 females). AD patients were recruited from the University of California San Francisco (UCSF) Memory and Aging Center. The diagnosis of AD was based on a comprehensive multidisciplinary evaluation that includes a clinical history and physical examination, a caregiver interview and a battery of neuropsychological tests (Kramer et al. 2003). All AD subjects met National Institute of Neurological Disorders and Stroke criteria for probable AD (McKhann et al. 1984) and had no significant comorbid medical, neurological, or psychiatric illnesses.

Neuropsychological Testing

All NC subjects underwent detailed cognitive testing in multiple domains to ensure normality. Normal cognitive performance was defined by creating composite scores in episodic memory (EM) (long delay free recall portion of the California Verbal Learning Test [CVLT] [Delis et al. 2000] and Wechsler Memory Scale [WMS-R] visual reproduction [Wechsler 1987b]), working memory (Wechsler Adult Intelligence Scale [WAIS-R] digit span backwards [Wechsler 1987a] and listening span total recall [Salhouse et al. 1991]), and frontal function (Trails *B* minus *A* [Reitan 1958] and Stroop total correct in 60 s [Zec 1986]) across a larger cohort of subjects ≥ 60 years old who underwent neuropsychological testing (198 subjects aged ≥ 60 were enrolled at the time of this study, mean age = 73.1 (7.6) and MMSE = 28.7 (1.7)). Subjects were considered ineligible if 1 composite score fell below 2 standard deviations (SDs) from our cohort defined age/gender/education-adjusted means. The individuals in this cohort were high functioning, such that a 2 SD cutoff yielded raw scores that were generally well within the range of age-adjusted normative data. These scores are thus more conservative than normative-derived cutoffs used in diagnosing mild cognitive impairment.

For subjects that had undergone multiple testing sessions, scores closest to the PET scan date were used (mean delay between PET and closest testing session was 3.93 (2.62) months, and the maximum delay was 10.2 months). Given the minimal amount of cognitive decline that may be expected in high PIB subjects in this short time period (Storandt et al. 2009), as well as the very slow rates of change in PIB uptake over time (Engler et al. 2006; Jack et al. 2009), this short delay is unlikely to have any effect on the results.

PET Acquisition

PIB was synthesized at the Lawrence Berkeley National Laboratory's (LBNL) Biomedical Isotope Facility using a published protocol and described in detail previously (Mathis et al. 2003; Mormino et al. 2009). PIB-PET imaging was performed using a Siemens ECAT EXACT HR PET scanner (Siemens Medical Systems) in 3D acquisition mode. Ten to fifteen mCi of PIB was injected into an antecubital vein. Dynamic acquisition frames were obtained as follows: 4×15 s, 8×30 s, 9×60 s, 2×180 s, 8×300 s, and 3×600 s (90 min total). A 10-min transmission scan for attenuation correction were obtained for each PIB scan. Filtered backprojected reconstructions were performed on the transmission and emission data to judge transmission alignment with each frame of emission data. In the case of misalignment, the transmission image was coregistered to that individual emission frame and then forward projected to create an attenuation correction file specific to that head position. PET data were reconstructed using an ordered subset expectation maximization algorithm with weighted attenuation. Images were smoothed with a 4-mm Gaussian kernel with scatter correction.

MRI Acquisition

MRI data on old and young NC subjects were collected at LBNL on a 1.5 T Magnetom Avanto System (Siemens Medical Systems) with a 12

channel head coil run in triple mode. The MRI session includes the following sequences (in order of acquisition): a T_2 -weighted fluid attenuated inversion recovery scan (FLAIR, axially acquired, time repetition [TR]/time echo [TE] = 9730/100 ms, flip angle = 150° , 0.80×0.80 -mm² in-plane resolution, 3.00-mm thickness with no gap), 3 T_1 -weighted volumetric magnetization prepared rapid gradient echo scans (MP-RAGE, axially acquired, TR/TE/time to inversion [TI] = 2110/3.58/1100 ms, flip angle = 15° , 1.00×1.00 -mm² in-plane resolution, 1.00-mm thickness with 50% gap), a T_1 structural scan in plane to the resting state scan (axially acquired, TR/TE = 500/10 ms, flip angle = 150° , 0.80×0.80 -mm² in-plane resolution, 3.5-mm thickness with 15% gap), and a resting state fMRI scan (acquired axially, TR/TE = 1890/50 ms, flip angle = 90° , 3.0×3.0 -mm² in-plane resolution, 3.5-mm³ thickness with 15% gap, 250 TRs total). The FLAIR scan was used to screen for stroke, whereas the in-plane T_1 and the MP-RAGE scans were used in subsequent processing steps. There was a mean time delay of 2.7 (6.3) months between PET and MRI scanning.

Resting state fMRI was not available for UCSF AD subjects. MP-RAGE scans for these subjects were used in the analysis of PIB-PET data. For 13 UCSF AD subjects, MP-RAGE scans were collected coronally on a 1.5 T Vision System (Siemens Medical Systems) with a quadrature head coil (TR/TE/TI = 10/7/300 ms, flip angle = 15° , 1.00×1.00 -mm² in-plane resolution, 1.40-mm slice thickness with no gap). For the remaining 9 UCSF AD subjects, MP-RAGE scans were collected sagittally on a Bruker MedSpec 4 T system with an 8 channel head coil (TR/TE/TI = 2300/3.37/950 ms, flip angle = 7° , 1.00×1.00 -mm² in-plane resolution, 1.00-mm slice thickness with no gap).

PET Preprocessing

PIB data were preprocessed using the SPM2 software package (<http://www.fil.ion.ucl.ac.uk/spm>). Realigned PIB frames corresponding to the first 20 min of acquisition were averaged and used to guide coregistration to the subject's structural MRI scan. Distribution volume ratios (DVRs) for PIB images were created using Logan graphical analysis with frames corresponding to 35–90 min postinjection and a gray matter masked cerebellum reference region (Logan et al. 1996; Price et al. 2005).

When applicable, PET images were coregistered to the subject's high-resolution structural scan and transformed to Montreal Neurological Institute (MNI) space using parameters defined from nonlinear alignment between the high-resolution structural scan and the MNI template (see the fMRI Preprocessing section). After normalization to template space, these PET images were smoothed an additional 8 mm, resulting in a total of 8.9 mm smoothing for these images.

Structural MRI Processing

MP-RAGE scans were processed as described previously using FreeSurfer version 4.3 (<http://surfer.nmr.mgh.harvard.edu/>) (Mormino et al. 2009). In brief, MP-RAGE scans were realigned and averaged to create a single high-contrast structural image. Anatomical masks relevant to PET processing were derived in each subject's native space using this analysis stream (Dale et al. 1999; Fischl et al. 2001; Fischl et al. 2002; Segonne et al. 2004). Specifically, a gray matter only cerebellum mask was used as a reference region for PIB and the mean PIB DVR value from a FreeSurfer derived cortical gray matter mask was extracted for each subject and used as a measure of global PIB uptake ("global PIB") and as a regressor in the voxelwise FC analysis. These global PIB values were highly correlated with the PIB index value used in our previous publication ($R^2 = 0.98$) (Mormino et al. 2009).

fMRI Preprocessing

fMRI data were processed using FMRIB Software Library (FSL) version 4.1 (<http://www.fmrib.ox.ac.uk/fsl>). Images were motion corrected, low-pass (2.8 s) and high-pass filtered (100 s), and smoothed with a 5-mm Gaussian kernel. To define the spatial transformation from fMRI space to MNI template space, a multistep registration procedure was employed. First, the mean fMRI image was linearly registered to the subject's in-plane T_1 structural image using 7 degrees of freedom. The in-plane T_1 image was then registered to the high-resolution structural

scan using 6 degrees of freedom. Finally, the high-resolution structural scan was nonlinearly aligned to the standard MNI 152 brain using FNIRT, and resulting parameters were used to transform fMRI data.

FC Analysis

FC analyses were conducted with FSL version 4.1 and adapted from the goodness of fit procedure described by Greicius et al. (2004). Supplementary Figure 1 provides a detailed schematic flow chart of the processing stream. A DMN template was defined using resting state fMRI data from the group of 17 young subjects. A seed in the posterior cingulate cortex (PCC; sphere of 8 mm centered at MNI coordinates -12, -50, 32) was transformed from template space into native fMRI space for each young subject. Additionally, nuisance regions were defined on the MNI template and transformed to native space (a white matter 8-mm spherical seed centered at MNI coordinates -24, -16, 36, a lateral ventricle mask drawn on the template, and a whole brain mask derived from segmenting the template brain and combining gray and white matter). Time series were extracted across all these regions and entered into a general linear model, and resulting contrast maps reflecting voxels correlated with the PCC time series (covarying the signal associated with white matter, lateral ventricle, and whole brain) were entered into a higher-level 1-sample *t*-test (height and extent joint threshold of $P < 0.05$, corrected). Based on evidence that the DMN may be “split” into posterior and anterior components with ICA (Damoiseaux et al. 2006, 2008), we excluded the anterior medial prefrontal cortex (mPFC) portion from this map and used the remaining posterior clusters as our template during the goodness of fit procedure (a “posterior” DMN template). This would ensure that posterior DMN components were selected for subjects with separable DMN components (27/44 subjects showed separable DMN components). A posterior rather than anterior template approach was employed because the posterior regions of the DMN have been implicated in EM processes (Andrews-Hanna et al. 2010) and show early dysfunction in AD (Minoshima et al. 1997; Killiany et al. 2002; Sorg et al. 2007; Thompson et al. 2007). Resting state data for each older NC was decomposed at the individual subject level using ICA with FSL’s Multivariate Exploratory Linear Optimized Decomposition into Independent Components (MELODIC) (Beckmann and Smith 2004). MELODIC isolates a multitude of components for each subject, and for each component, voxels are assigned a *z*-score that reflects the extent to which that voxel’s time series is correlated with the time series associated with the specific component. A goodness of fit procedure was applied to spatially normalized *z*-maps for each subject to determine which component most closely resembled the DMN template (average *z*-score of voxels within the template minus average *z*-score of voxels outside the template; *z*-values from the removed mPFC area were excluded from this calculation to ensure that high mPFC connectivity did not inflate the average value “outside” the template). The *z*-map for the best-fit component for each subject was used in subsequent higher-level analyses.

Statistical Analyses

Correlations between global PIB and demographic variables were completed using the statistical programming language R version 2.8 (<http://www.r-project.org/>). Partial correlation coefficients (*r*) were reported for relationships between global PIB and EM/MMSE (controlling for demographic predictors). Caret version 5 was used to display voxelwise results (<http://brainvis.wustl.edu/wiki/index.php/Caret>About>).

Spatial overlap between the DMN and the PIB uptake was qualitatively examined by overlaying statistical maps. The DMN FC map was derived from a 1-sample *t*-test of DMN best-fit components from the elderly NC group, whereas the PIB uptake map was derived from contrasting low PIB NC with high PIB NC DVR images (defined with a median split of global PIB values). The FC map was thresholded at $P < 0.001$ and $k = 100$, uncorrected and the PIB map was thresholded at $P < 0.0002$ and $k = 100$, uncorrected, binarized, and overlaid upon a 3D rendered brain.

Within the NC group, global PIB was treated as a continuous value and regressed against voxelwise DMN FC using permutation testing

with FSL’s Randomise (using 5000 permutations, <http://www.fmrib.ox.ac.uk/fsl/randomise/>). This analysis was restricted to the voxels that were significant in the DMN 1-sample *t*-test of elderly NC subjects (thresholded at $P < 0.001$ and $k = 100$, uncorrected; this mask is displayed in Fig. 1). Age, gender, and education were controlled for in this analysis, and results were considered significant at $P < 0.05$ and $k = 50$, uncorrected. Cluster size, maximum *t*-statistic/*P*-value, and peak MNI coordinates for significant regions are reported.

To explore focal PIB uptake within regions showing a relationship between FC and global PIB, region of interest (ROI) analyses were completed with R. ROIs were created from the primary FC voxelwise results by casting an 8-mm sphere around the voxel with the highest *t*-value in a subset of significant clusters (voxels showing the strongest relationship between FC and global PIB). PIB values from these ROIs were extracted from spatially normalized PET images. A repeated measures analysis of variance (ANOVA) was conducted with PIB DVR values as the dependent variable, group (AD and NC) as a between-subjects factor and ROI as a within-subjects factor. Main effects of group and ROI were investigated further with post hoc contrasts [1) AD vs. NC for each ROI and 2) each ROI vs. global PIB controlling for diagnosis]. Within the NC group, mean FC was extracted from these ROIs and regressed against EM. Age, gender, and education were controlled for in each model. Results were considered significant at $P < 0.05$.

Results

Demographics

Demographics for elderly NC subjects are listed in Table 1. There was a significant relationship between global PIB and gender ($P = 0.03$; higher PIB in females) and a trend between global PIB and age ($P = 0.08$; higher PIB in older subjects).

Spatial Overlap of DMN and A β Deposition

Results from the 1-sample *t*-test of best-fit components of the DMN in elderly NC revealed significant clusters in medial and lateral prefrontal cortex, posteromedial cortex (precuneus/posterior cingulate and retrosplenial cortices), lateral parietal, middle temporal, and medial temporal cortices. Overlap between the DMN and the A β deposition is displayed in Figure 1. There is a large degree of convergence between DMN FC and PIB uptake,

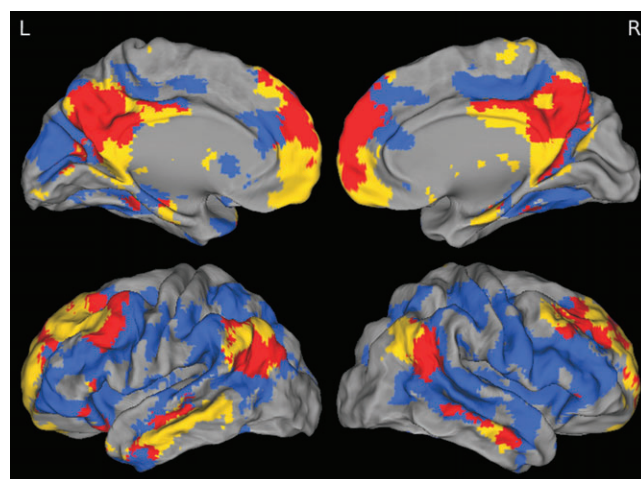


Figure 1. DMN FC and global PIB uptake overlap. One sample *t*-test of DMN best-fit components (yellow), 2-sample *t*-test between high and low PIB subjects (blue), and overlap (red) are displayed. These maps highlight congruence and incongruence between the DMN and the brain regions showing high levels of A β deposition. The greatest amount of overlap is in precuneus/posterior cingulate, medial prefrontal, and angular gyri. Although PIB uptake is more diffuse than DMN, there is minimal overlap in retrosplenial and medial temporal portions of the DMN.

most notably in the precuneus/posterior cingulate, angular gyri, and mPFC, whereas limited overlap was present in the medial temporal lobe.

Global PIB Versus DMN FC

To examine the relationship between A β deposition and DMN FC, global PIB values were regressed against voxelwise DMN FC maps (Fig. 2 and Table 2). Multiple regions in the posteromedial cortex showed reduced FC with increased levels of PIB (precuneus, posterior cingulate, and retrosplenial cortex). Elevated PIB was also associated with decreased DMN FC in ventral mPFC (vmPFC), right angular gyrus, and the left middle and superior frontal gyri. Additionally, there were areas of the DMN that showed increased FC with higher levels of global PIB (right dorsal prefrontal [R dPFC], left anterior medial prefrontal [L amPFC], and left middle temporal cortices). This analysis was repeated using PIB data that was corrected for partial volume effects as described in our previous publication (Mormino et al. 2009), and results did not differ (see Supplementary Figure 2).

Given the novel finding of increased DMN FC with elevated PIB in NC, we conducted a series of seed based analyses similar to the methods employed in the 2 previously published papers examining DMN FC and PIB in NC (Hedden et al. 2009; Sheline et al. 2010). These analyses were consistent with the results obtained using ICA (Supplementary Analysis 1, Supplementary Figures 3 and 4).

Colocalization of PIB Uptake and A β -Related DMN FC Differences

To further explore A β -related DMN FC differences, the 6 ROIs showing the strongest negative and positive correlation with

PIB (Table 2 and Supplementary Figure 5) were selected from the ICA voxelwise analysis: ROIs in the left precuneus (L Precun), vmPFC, and left retrosplenial cortex (L RSC) that showed reduced FC with increased global PIB, as well as ROIs in R dPFC, L amPFC, and left middle temporal gyrus (L MTG) that showed heightened FC with increased global PIB. Average PIB values were extracted from these ROIs and entered into a repeated measures ANOVA with diagnosis (AD, NC) as a between-subjects factor and ROI as a within-subjects factor (values across all ROIs are plotted in Fig. 3). To understand where PIB is elevated in NC and how this elevation differs from AD and across regions, this analysis was restricted to high PIB NC subjects (determined via a median split within the NC group). This analysis revealed significant main effects of both diagnosis ($F = 33.132$, $P < 0.001$) and ROI ($F = 76.372$, $P < 0.001$). Post hoc contrasts between AD and NC revealed significant elevation in AD in all ROIs (Supplementary Table 1). To understand whether there was an appreciable pattern of uptake amongst these ROIs, each ROI was contrasted against global PIB (controlling for diagnosis). This analysis did not reveal concordance between the PIB uptake and the direction

Table 1
Cohort demographics and correlations with global PIB

		Relationship with global PIB
<i>N</i>	44	—
Age	74.6 (6.3)	$r = 0.27$, $t = 1.79$, $P = 0.08$
Gender	29 females, 15 males	$r = -0.32$, $t = -2.20$, $P = 0.03$
Education	17.1 (1.9)	$r = -0.13$, $t = -0.82$, $P = 0.42$
MMSE	29.0 (1.1)	$r = -0.08$, $t = -0.55$, $P = 0.58$
EM	0.22 (0.71)	$r = -0.19$, $t = -1.31$, $P = 0.20$

Mean and SDs are listed for continuous variables. Demographic variables (age, gender, and education) were controlled when examining relationships between global PIB and MMSE/EM. Significant relationships and trends are bolded.

Table 2
Results from primary voxelwise analysis

Location	Max <i>T</i>	Max <i>P</i>	Voxels	<i>x</i>	<i>y</i>	<i>z</i>
Negative correlations						
<i>L precun</i>	3.68	0.0002	692	4	68	26
<i>Bilateral vmPFC</i>	3.55	0.001	113	2	36	-24
<i>L RSC</i>	3.27	0.001	133	12	48	2
<i>L PCC</i>	3.24	0.0002	69	0	26	26
R middle frontal cortex	3.19	0.001	169	28	22	40
R angular gyrus	3.06	0.001	71	64	46	16
R RSC	3	0.004	50	22	50	4
<i>Bilateral vmPFC</i>	2.93	0.001	226	0	52	-20
R angular/occipital cortex	2.84	0.001	67	46	62	36
L superior frontal gyrus	2.64	0.006	63	18	30	44
R posterior cingulate	2.31	0.011	52	6	44	16
R precun	2.11	0.017	54	10	66	30
Positive correlations						
<i>R dPFC</i>	3.91	0.001	162	14	42	34
<i>L amPFC</i>	3.37	0.002	199	8	66	14
<i>L MTG</i>	3.11	0.002	51	-66	-44	-8

Regions showing negative and positive relationships between global PIB and DMN FC are listed. Values corresponding to the voxel within each cluster showing the strongest association between PIB and DMN FC are listed, as well as cluster size. Italics indicate regions selected for additional ROI analyses.

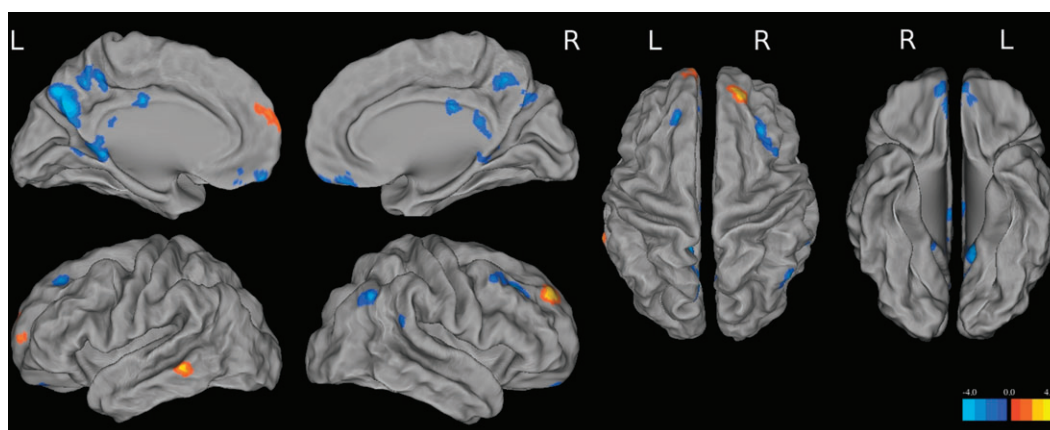


Figure 2. *t*-Maps from voxelwise analysis correlating global PIB with DMN FC. Cool colors reflect a negative relationship, whereas warm colors reflect a positive relationship between global PIB and DMN FC.

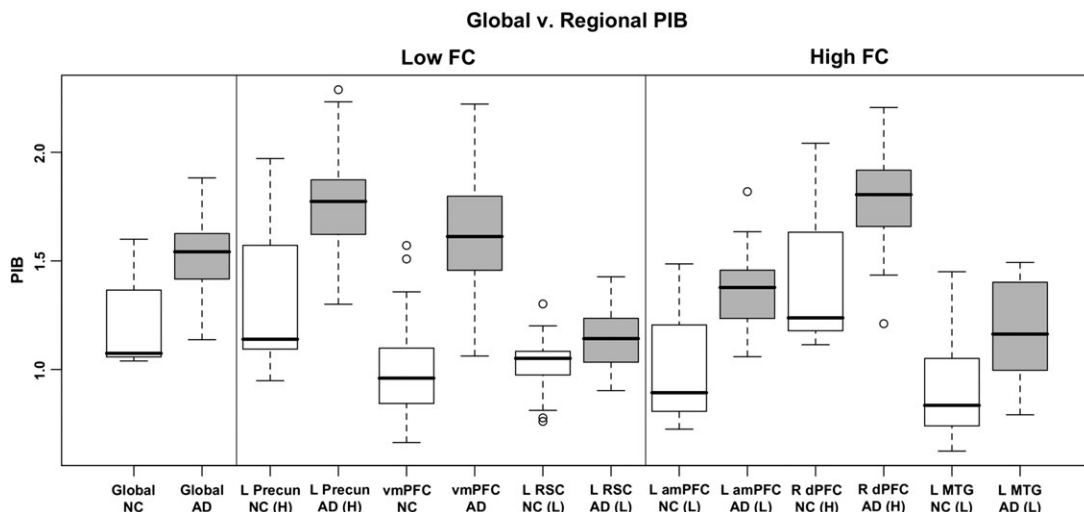


Figure 3. Boxplots of global and regional PIB values in high PIB NC (white boxes) and AD (gray boxes). Although AD subjects show heightened PIB, overlap between AD and NC suggests the early A β deposition in NC. Despite low PIB uptake in L RSC, L amPFC, and L MTG, these regions show FC changes with increased levels of global PIB.

of the ROI's relationship between global PIB and FC (i.e., 1 region showing decreased FC with elevated global PIB was significantly higher than global PIB (L Precun), where 1 region was significantly lower (L RSC); additionally, 1 region showing increased FC with more PIB was significantly higher than global PIB (R dPFC), whereas 2 regions were lower (L amPFC and L MTG); see Supplementary Table 1).

To continue exploring a potential relevance of regional PIB uptake, we conducted an additional analysis to determine if focal PIB across any ROI shows heightened relevance to DMN FC (Supplementary Analysis 2). Specifically, it is possible that intraregional PIB is strongly related with FC in specific DMN areas, or that PIB uptake in 1 region is a strong predictor of FC changes in distant DMN regions. To investigate this possibility, we conducted a series of regression analyses relating FC to PIB within each ROI and across ROIs. This analysis did not reveal evidence for a specific impact of regional PIB—areas that show relationships with increased PIB tend to do so across multiple PIB ROIs and to a similar extent to the correlation with global PIB (Supplementary Table 2). It is possible that the high covariance in PIB uptake across regions makes regional contributions difficult to disentangle (Supplementary Table 3).

Relationships between A β -Related DMN FC Differences and EM

EM was not correlated with global PIB ($t = -1.31$, $P = 0.20$). There was a trend for a positive relationship between EM and DMN FC in RSC ($t = 1.82$, $P = 0.08$), and no other relationships were found with FC from any other ROI.

Discussion

In this study, we found relationships between global PIB uptake and DMN resting state FC in a group of elderly cognitively intact individuals. Specifically, increased A β deposition was associated with decreased DMN FC in multiple posteromedial regions (precuneus/posterior cingulate and retrosplenial cortices), as well as vmPFC, right angular gyrus, and the left middle and superior frontal gyri. These regions showing decreased

DMN FC are consistent with previous studies combining resting state fMRI and PIB-PET imaging in NC (Hedden et al. 2009; Sheline et al. 2010) and have furthermore shown changes across multiple imaging modalities, demonstrating both glucose hypometabolism and atrophy in early AD (Minoshima et al. 1997; de Leon et al. 2001; Killiany et al. 2002; Greicius et al. 2004; Sorg et al. 2007; Thompson et al. 2007). Interestingly, we also found that elevated PIB was associated with increased DMN FC in R dPFC, L amPFC, and left middle temporal cortices, which may reflect either compensatory processes or aberrant activity. Importantly, this dissociation was consistent across multiple analytic approaches, suggesting that these results are not a methodological artifact. Furthermore, relationships between imaging measures and EM were either absent or weak, suggesting that A β -related changes in DMN FC occur in the absence of overt cognitive deficits.

Differential Relationships between DMN FC and A β May Reflect Region-Specific Properties

The results identified in this study suggest that regions within the DMN respond differently to high levels of A β deposition, and it is possible that the impact of this pathology is modified by region-specific properties. Interestingly, the reported pattern of A β -related FC differences aligns with proposed subsystems of the DMN (Greicius et al. 2009; Andrews-Hanna et al. 2010). Andrews-Hanna et al. (2010) recently described 2 distinct DMN subsystems that interact via the PCC and the anterior mPFC (the "midline core"): a medial temporal lobe subsystem involved in EM processes and a dorsal mPFC subsystem involved in self-relevant processes. Interestingly, the pattern of A β -related decreased FC identified in our study shows substantial overlap with the medial temporal lobe subsystem (retrosplenial cortices, vmPFC, angular gyrus as well as regions in posteromedial cortex that may be considered part of the midline core). Furthermore, the pattern of A β -related increased FC overlaps with the dorsal mPFC subsystem (dorsal PFC and lateral temporal cortex, as well as a region in the anterior mPFC that may be considered part of the midline core).

This spatial dissociation of A β -related FC changes suggests differential effects on DMN subsystems. The pattern of decreased FC in the EM/medial temporal subsystem suggests heightened vulnerability of this DMN subsystem to A β deposition and is consistent with the trend we observed between decreased RSC FC and lower EM performance in our subjects. These results are consistent with 2 recently published resting state studies examining A β in aging (Hedden et al. 2009; Sheline et al. 2010) as well as numerous reports of brain changes to the medial temporal subsystem in AD; it is possible that disconnection in these regions eventually leads to more severe changes (such as neuronal atrophy) and underlies the EM deficits observed in AD.

The pattern of increased FC observed in this study may be compensatory, excitatory, or a combination of both. Although the biological relevance of increased FC during rest is unclear, recent reports have suggested a compensatory role of elevated FC in subjects at risk for AD (Filippini et al. 2009; Qi et al. 2010). In the context of our study, it is possible that increased FC may compensate for failing medial temporal subsystem regions (Reuter-Lorenz 2002), such that the DMN has a compensatory “shift” toward the dorsal mPFC subsystem as the medial temporal subsystem is negatively affected by A β . Consistent with potential compensatory capabilities, the PFC in particular appears less vulnerable to A β toxicity than posterior DMN regions, with PFC neuronal dysfunction associated with late stages of AD (Langbaum et al. 2009) despite evidence of early PFC A β deposition (Mintun et al. 2006). It has been proposed that brain regions show different time delays between initiating A β deposition and resulting regional abnormalities, with speculation that PFC has the longest delay (Jack et al. 2010). Given these characteristics, the PFC is a potential source of compensation in response to A β accumulation, in particular the dorsal and anterior mPFC portion of the DMN. A compensatory shift toward the dorsal mPFC system may reflect neuronal plasticity or the potential to deploy new cognitive strategies in the face of A β deposition. Although not tested in this study, it is possible that high PIB subjects have adopted new strategies that rely on cognitive processes subserved by the dorsal mPFC subsystem, such as self-referential processing during encoding (Andrews-Hanna et al. 2010). Future studies that examine encoding strategies in aged individuals with high levels of A β deposition will offer insight into this potential source of neuronal compensation.

Conversely, FC increases may reflect an early aberrant excitatory response to A β . Interestingly, a recent task-related fMRI study reported a failure to deactivate medial prefrontal, precuneus/posterior cingulate, and lateral temporal cortices during successful EM encoding in elderly adults with elevated PIB uptake (Sperling et al. 2009). The authors proposed that A β deposition may cause aberrant modulation in these DMN regions, and it is possible that persistent activation in these areas reflects the aberrant spiking activity that has been seen with *in vitro* models and which may be excitotoxic (Palop et al. 2007). Although it is difficult to reconcile the results of task-related fMRI and resting state FC studies, the fact that increases within DMN regions were observed in both contexts is intriguing. Inability to modulate DMN regions may additionally facilitate a cyclical process that promotes further A β production (Cirrito et al. 2005) and eventually hypoactivation. This is consistent with observations that in AD patients regions in the dmPFC subsystem display the same pattern of DMN FC

decreases that we identified in the medial temporal lobe subsystem in normal elderly (Greicius et al. 2004). In this context, compensatory and aberrant hyperactivation are not necessarily mutually exclusive; it is possible that compensatory responses may ultimately lead to downstream activity reductions as neurons undergo excitotoxicity.

Global Versus Regional A β Deposition

The results presented in our primary analysis focused on relationships between global A β levels and FC in DMN regions. It is possible that differential deposition of A β in different subsystems or nodes of the DMN could be responsible for our reported regions of increased, as opposed to decreased FC. We explored these possibilities by examining the pattern of PIB uptake within regions showing strong relationships with global PIB and identified significant elevation in PIB uptake in AD compared with NC across all ROIs. Interestingly, we found that ROIs showing significant elevation compared with our global measure of PIB were present for ROIs showing both increased FC (R dPFC) and decreased FC (L Precun). The same pattern was observed for ROIs with significantly lower PIB than the global measure (increased FC: L ampFC and L MTG; decreased FC: L RSC). These findings were independent of diagnosis, suggesting that these low ROIs remain low even in the context of AD (when amyloid levels are much higher and more neuronal dysfunction has occurred).

To address the possibility of heightened relevance of amyloid in individual ROIs, we directly compared intraregional and interregional relationships in DMN ROIs between PIB and FC. This analysis did not provide evidence for relationships that were specific to regional PIB uptake (areas that show relationships between FC and PIB tend to do so across multiple PIB ROIs). However, it is likely that high covariance amongst all regions made such a relationship difficult to detect.

It is possible that these null findings may be attributable to an inability to capture focal DMN changes before widespread A β deposition occurred. In particular, the precuneus and PCC are likely candidates for focal effects of A β since these regions have dense connections within and beyond the DMN (Hagmann et al. 2008; Buckner et al. 2009), and it is possible that disruption in either of these regions would affect other DMN regions. Studies that focus on earlier stages (i.e., involving younger samples) may be able to capture initial A β deposition before widespread highly correlated uptake is observed and will help clarify whether regional PIB has an impact. A further possibility is that fibrillar A β is not a primary pathological cause of disrupted DMN FC. It is possible that regional levels of soluble A β or neurofibrillary tangles may cause connectivity decreases within DMN nodes. Since PIB-PET binds predominately to fibrillar forms of A β (Ikonomic et al. 2008), our data are unable address these potential relationships.

Overall, although the mechanism by which heightened A β levels affect the DMN in a widespread fashion remains unclear, our data suggest that A β -related DMN changes are not exclusively related to focal A β deposition but rather reflect the interaction of a global pathological process with properties of the distinct DMN components (i.e., nodes in the EM subsystem of the DMN may show heightened vulnerability to amyloid deposition, whereas nodes in the dmPFC subsystem may show compensatory capabilities).

Relationships with Episodic Memory

Studies using PIB-PET imaging in NC have failed to find a consistent relationship between elevated PIB and concurrent EM (Pike et al. 2007; Jack et al. 2008; Mormino et al. 2009). However, recent studies have shown that elevated PIB is associated with subsequent cognitive decline in NC (Morris et al. 2009; Storandt et al. 2009). According to the timeline posited by Jack et al. 2010, the relationship between EM and A β deposition within NC may be influenced by mediating factors (Jack et al. 2010), which likely obscures potential correlations between EM and A β . Potential mediating factors include downstream changes caused by A β toxicity, such as neurofibrillary tangle deposition and neuronal loss (Bennett et al. 2004; Mormino et al. 2009).

Relationships with EM investigated in this study were either null or weak. The correlation between global PIB and EM was insignificant, whereas there was a trend with DMN FC in L RSC. This pattern is consistent with FC changes representing downstream effects of A β toxicity, but the weak associations do not allow us to draw conclusions about the potential mediation of PIB effects on EM by DMN FC. Overall, our results emphasize that A β deposition and corresponding brain changes occur in subjects without overt cognitive deficits.

Limitations

This study has several limitations. PIB does not bind to diffuse plaques or soluble A β (Ikonomovic et al. 2008), which may show more relevance than fibrillar A β in evaluating the regional impact of this pathology on DMN FC. The statistical thresholds used in our voxelwise analyses were liberal. However, the pattern of DMN FC decreases is consistent with a large body of literature that suggests selective vulnerability of posterior EM-related regions in early AD development. Furthermore, the ability to detect regional effects of amyloid may be limited by the high covariance of PIB values across brain regions—studies with more subjects will be necessary to untangle potential relationships with regional deposition. Another limitation is reliance on cross-sectional cognitive testing scores. Longitudinal cognitive data may be a superior indicator of preclinical AD and show higher correlations with PIB and resting state DMN FC measures. Lastly, our analysis was limited to cognitively normal elderly individuals; a group in which small effect sizes are expected and studies with larger numbers are warranted.

Supplementary Material

Supplementary material can be found at: <http://www.cercor.oxfordjournals.org/>

Funding

National Institutes of Health (AG027859, AG032814); Alzheimer's Association (ZEN-08-87090).

Notes

Conflict of Interest: None declared.

References

Andrews-Hanna JR, Reidler JS, Sepulcre J, Poulin R, Buckner RL. 2010. Functional-anatomic fractionation of the brain's default network. *Neuron*. 65:550–562.

- Arnold SE, Hyman BT, Flory J, Damasio AR, Van Hoesen GW. 1991. The topographical and neuroanatomical distribution of neurofibrillary tangles and neuritic plaques in the cerebral cortex of patients with Alzheimer's disease. *Cereb Cortex*. 1:103–116.
- Beckmann CF, Smith SM. 2004. Probabilistic independent component analysis for functional magnetic resonance imaging. *IEEE Trans Med Imaging*. 23:137–152.
- Bennett DA, Schneider JA, Arvanitakis Z, Kelly JF, Aggarwal NT, Shah RC, Wilson RS. 2006. Neuropathology of older persons without cognitive impairment from two community-based studies. *Neurology*. 66:1837–1844.
- Bennett DA, Schneider JA, Wilson RS, Bienias JL, Arnold SE. 2004. Neurofibrillary tangles mediate the association of amyloid load with clinical Alzheimer disease and level of cognitive function. *Arch Neurol*. 61:378–384.
- Bourgeat P, Chetelat G, Villemagne VL, Fripp J, Raniga P, Pike K, Acosta O, Szoek C, Ourselin S, Ames D, et al. 2010. Beta-amyloid burden in the temporal neocortex is related to hippocampal atrophy in elderly subjects without dementia. *Neurology*. 74:121–127.
- Buckner RL, Andrews-Hanna JR, Schacter DL. 2008. The brain's default network: anatomy, function, and relevance to disease. *Ann N Y Acad Sci*. 1124:1–38.
- Buckner RL, Sepulcre J, Talukdar T, Krienen FM, Liu H, Hedden T, Andrews-Hanna JR, Sperling RA, Johnson KA. 2009. Cortical hubs revealed by intrinsic functional connectivity: mapping, assessment of stability, and relation to Alzheimer's disease. *J Neurosci*. 29:1860–1873.
- Buckner RL, Snyder AZ, Shannon BJ, LaRossa G, Sachs R, Fotenos AF, Sheline YI, Klunk WE, Mathis CA, Morris JC, et al. 2005. Molecular, structural, and functional characterization of Alzheimer's disease: evidence for a relationship between default activity, amyloid, and memory. *J Neurosci*. 25:7709–7717.
- Buckner RL, Vincent JL. 2007. Unrest at rest: default activity and spontaneous network correlations. *Neuroimage*. 37:1091–1096; discussion 1097–1099.
- Cirrito JR, Yamada KA, Finn MB, Sloviter RS, Bales KR, May PC, Schoepp DD, Paul SM, Mennerick S, Holtzman DM. 2005. Synaptic activity regulates interstitial fluid amyloid-beta levels in vivo. *Neuron*. 48:913–922.
- Dale AM, Fischl B, Sereno MI. 1999. Cortical surface-based analysis. I. Segmentation and surface reconstruction. *Neuroimage*. 9:179–194.
- Damoiseaux JS, Beckmann CF, Arigita EJ, Barkhof F, Scheltens P, Stam CJ, Smith SM, Rombouts SA. 2008. Reduced resting-state brain activity in the "default network" in normal aging. *Cereb Cortex*. 18:1856–1864.
- Damoiseaux JS, Rombouts SA, Barkhof F, Scheltens P, Stam CJ, Smith SM, Beckmann CF. 2006. Consistent resting-state networks across healthy subjects. *Proc Natl Acad Sci U S A*. 103:13848–13853.
- Davis DG, Schmitt FA, Wekstein DR, Markesbery WR. 1999. Alzheimer neuropathologic alterations in aged cognitively normal subjects. *J Neuropathol Exp Neurol*. 58:376–388.
- de Leon MJ, Convit A, Wolf OT, Tarshish CY, DeSanti S, Rusinek H, Tsui W, Kandil E, Scherer AJ, Roche A, et al. 2001. Prediction of cognitive decline in normal elderly subjects with 2-[(18)F]fluoro-2-deoxy-D-glucose/positron-emission tomography (FDG/PET). *Proc Natl Acad Sci U S A*. 98:10966–10971.
- Delis D, Kramer J, Kaplan E, Ober B. 2000. California verbal learning test. San Antonio (TX): The Psychological Corporation.
- Dickerson BC, Bakkour A, Salat DH, Feczko E, Pacheco J, Greve DN, Grodstein F, Wright CI, Blacker D, Rosas HD, et al. 2009. The cortical signature of Alzheimer's disease: regionally specific cortical thinning relates to symptom severity in very mild to mild AD dementia and is detectable in asymptomatic amyloid-positive individuals. *Cereb Cortex*. 19:497–510.
- Engler H, Forsberg A, Almkvist O, Blomquist G, Larsson E, Savitcheva I, Wall A, Ringheim A, Langstrom B, Nordberg A. 2006. Two-year follow-up of amyloid deposition in patients with Alzheimer's disease. *Brain*. 129:2856–2866.
- Filippini N, MacIntosh BJ, Hough MG, Goodwin GM, Frisoni GB, Smith SM, Matthews PM, Beckmann CF, Mackay CE. 2009. Distinct

- patterns of brain activity in young carriers of the APOE-epsilon4 allele. *Proc Natl Acad Sci U S A*. 106:7209-7214.
- Fischl B, Liu A, Dale AM. 2001. Automated manifold surgery: constructing geometrically accurate and topologically correct models of the human cerebral cortex. *IEEE Trans Med Imaging*. 20:70-80.
- Fischl B, Salat DH, Busa E, Albert M, Dieterich M, Haselgrove C, van der Kouwe A, Killiany R, Kennedy D, Klaveness S, et al. 2002. Whole brain segmentation: automated labeling of neuroanatomical structures in the human brain. *Neuron*. 33:341-355.
- Fox MD, Raichle ME. 2007. Spontaneous fluctuations in brain activity observed with functional magnetic resonance imaging. *Nat Rev Neurosci*. 8:700-711.
- Fox MD, Snyder AZ, Vincent JL, Corbetta M, Van Essen DC, Raichle ME. 2005. The human brain is intrinsically organized into dynamic, anticorrelated functional networks. *Proc Natl Acad Sci U S A*. 102:9673-9678.
- Greicius MD, Krasnow B, Reiss AL, Menon V. 2003. Functional connectivity in the resting brain: a network analysis of the default mode hypothesis. *Proc Natl Acad Sci U S A*. 100:253-258.
- Greicius MD, Srivastava G, Reiss AL, Menon V. 2004. Default-mode network activity distinguishes Alzheimer's disease from healthy aging: evidence from functional MRI. *Proc Natl Acad Sci U S A*. 101:4637-4642.
- Greicius MD, Supekar K, Menon V, Dougherty RF. 2009. Resting-state functional connectivity reflects structural connectivity in the default mode network. *Cereb Cortex*. 19:72-78.
- Hagmann P, Cammoun L, Gigandet X, Meuli R, Honey CJ, Wedeen VJ, Sporns O. 2008. Mapping the structural core of human cerebral cortex. *PLoS Biol*. 6:e159.
- Hedden T, Van Dijk KR, Becker JA, Mehta A, Sperling RA, Johnson KA, Buckner RL. 2009. Disruption of functional connectivity in clinically normal older adults harboring amyloid burden. *J Neurosci*. 29:12686-12694.
- Hulette CM, Welsh-Bohmer KA, Murray MG, Saunders AM, Mash DC, McIntyre LM. 1998. Neuropathological and neuropsychological changes in "normal" aging: evidence for preclinical Alzheimer disease in cognitively normal individuals. *J Neuropathol Exp Neurol*. 57:1168-1174.
- Ikonomovic MD, Klunk WE, Abrahamson EE, Mathis CA, Price JC, Tsopelas ND, Lopresti BJ, Ziolkowski S, Bi W, Paljug WR, et al. 2008. Post-mortem correlates of in vivo PiB-PET amyloid imaging in a typical case of Alzheimer's disease. *Brain*. 131:1630-1645.
- Jack CR, Knopman DS, Jagust WJ, Shaw LM, Aisen PS, Weiner MW, Petersen RC, Trojanowski JQ. 2010. Hypothetical model of dynamic biomarkers of the Alzheimer's pathological cascade. *Lancet Neurol*. 9:119-128.
- Jack CR, Jr, Lowe VJ, Senjem ML, Weigand SD, Kemp BJ, Shiung MM, Knopman DS, Boeve BF, Klunk WE, Mathis CA, et al. 2008. 11C PiB and structural MRI provide complementary information in imaging of Alzheimer's disease and amnesic mild cognitive impairment. *Brain*. 131:665-680.
- Jack CR, Jr, Lowe VJ, Weigand SD, Wiste HJ, Senjem ML, Knopman DS, Shiung MM, Gunter JL, Boeve BF, Kemp BJ, et al. 2009. Serial PiB and MRI in normal, mild cognitive impairment and Alzheimer's disease: implications for sequence of pathological events in Alzheimer's disease. *Brain*. 132:1355-1365.
- Killiany RJ, Hyman BT, Gomez-Isla T, Moss MB, Kikinis R, Jolesz F, Tanzi R, Jones K, Albert MS. 2002. MRI measures of entorhinal cortex vs hippocampus in preclinical AD. *Neurology*. 58:1188-1196.
- Klunk WE, Engler H, Nordberg A, Wang Y, Blomqvist G, Holt DP, Bergstrom M, Savitcheva I, Huang GF, Estrada S, et al. 2004. Imaging brain amyloid in Alzheimer's disease with Pittsburgh compound-B. *Ann Neurol*. 55:306-319.
- Knopman DS, Parisi JE, Salviati A, Floriach-Robert M, Boeve BF, Ivnik RJ, Smith GE, Dickson DW, Johnson KA, Petersen LE, et al. 2003. Neuropathology of cognitively normal elderly. *J Neuropathol Exp Neurol*. 62:1087-1095.
- Kramer JH, Jurik J, Sha SJ, Rankin KP, Rosen HJ, Johnson JK, Miller BL. 2003. Distinctive neuropsychological patterns in frontotemporal dementia, semantic dementia, and Alzheimer disease. *Cogn Behav Neurol*. 16:211-218.
- Langbaum JB, Chen K, Lee W, Reschke C, Bandy D, Fleisher AS, Alexander GE, Foster NL, Weiner MW, Koeppe RA, et al. 2009. Categorical and correlational analyses of baseline fluorodeoxyglucose positron emission tomography images from the Alzheimer's Disease Neuroimaging Initiative (ADNI). *Neuroimage*. 45:1107-1116.
- Logan J, Fowler JS, Volkow ND, Wang GJ, Ding YS, Alexoff DL. 1996. Distribution volume ratios without blood sampling from graphical analysis of PET data. *J Cereb Blood Flow Metab*. 16:834-840.
- Mathis CA, Wang Y, Holt DP, Huang GF, Debnath ML, Klunk WE. 2003. Synthesis and evaluation of 11C-labeled 6-substituted 2-arylbenzothiazoles as amyloid imaging agents. *J Med Chem*. 46:2740-2754.
- McKhann G, Drachman D, Folstein M, Katzman R, Price D, Stadlan EM. 1984. Clinical diagnosis of Alzheimer's disease: report of the NINCDS-ADRDA Work Group under the auspices of Department of Health and Human Services Task Force on Alzheimer's Disease. *Neurology*. 34:939-944.
- Minoshima S, Giordani B, Berent S, Frey KA, Foster NL, Kuhl DE. 1997. Metabolic reduction in the posterior cingulate cortex in very early Alzheimer's disease. *Ann Neurol*. 42:85-94.
- Mintun MA, Larossa GN, Sheline YI, Dence CS, Lee SY, Mach RH, Klunk WE, Mathis CA, DeKosky ST, Morris JC. 2006. [11C]PiB in a nondemented population: potential antecedent marker of Alzheimer disease. *Neurology*. 67:446-452.
- Mormino EC, Kluth JT, Madison CM, Rabinovici GD, Baker SL, Miller BL, Koeppe RA, Mathis CA, Weiner MW, Jagust WJ. 2009. Episodic memory loss is related to hippocampal-mediated beta-amyloid deposition in elderly subjects. *Brain*. 132:1310-1323.
- Morris JC, Roe CM, Grant EA, Head D, Storandt M, Goate AM, Fagan AM, Holtzman DM, Mintun MA. 2009. Pittsburgh compound B imaging and prediction of progression from cognitive normality to symptomatic Alzheimer disease. *Arch Neurol*. 66:1469-1475.
- Palop JJ, Chin J, Roberson ED, Wang J, Thwin MT, Bien-Ly N, Yoo J, Ho KO, Yu GQ, Kreitzer A, et al. 2007. Aberrant excitatory neuronal activity and compensatory remodeling of inhibitory hippocampal circuits in mouse models of Alzheimer's disease. *Neuron*. 55:697-711.
- Pike KE, Savage G, Villemagne VL, Ng S, Moss SA, Maruff P, Mathis CA, Klunk WE, Masters CL, Rowe CC. 2007. Beta-amyloid imaging and memory in non-demented individuals: evidence for preclinical Alzheimer's disease. *Brain*. 130:2837-2844.
- Price JC, Klunk WE, Lopresti BJ, Lu X, Hoge JA, Ziolkowski SK, Holt DP, Meltzer CC, DeKosky ST, Mathis CA. 2005. Kinetic modeling of amyloid binding in humans using PET imaging and Pittsburgh compound-B. *J Cereb Blood Flow Metab*. 25:1528-1547.
- Price JL, Morris JC. 1999. Tangles and plaques in nondemented aging and "preclinical" Alzheimer's disease. *Ann Neurol*. 45:358-368.
- Qi Z, Wu X, Wang Z, Zhang N, Dong H, Yao L, Li K. 2010. Impairment and compensation coexist in amnesic MCI default mode network. *Neuroimage*. 50:48-55.
- Rabinovici GD, Jagust WJ. 2009. Amyloid imaging in aging and dementia: testing the amyloid hypothesis in vivo. *Behav Neurol*. 21:117-128.
- Raichle ME, Snyder AZ. 2007. A default mode of brain function: a brief history of an evolving idea. *Neuroimage*. 37:1083-1090discussion 1097-1089.
- Reitan RM. 1958. Validity of the Trailmaking Test as an indication of organic brain damage. *Percept Mot Skills*. 8:271-276.
- Reuter-Lorenz P. 2002. New visions of the aging mind and brain. *Trends Cogn Sci*. 6:394.
- Salthouse TA, Babcock RL, Shaw RJ. 1991. Effects of adult age on structural and operational capacities in working memory. *Psychol Aging*. 6:118-127.
- Savva GM, Wharton SB, Ince PG, Forster G, Matthews FE, Brayne C. 2009. Age, neuropathology, and dementia. *N Engl J Med*. 360:2302-2309.
- Segonne F, Dale AM, Busa E, Glessner M, Salat D, Hahn HK, Fischl B. 2004. A hybrid approach to the skull stripping problem in MRI. *Neuroimage*. 22:1060-1075.

- Sheline YI, Raichle ME, Snyder AZ, Morris JC, Head D, Wang S, Mintun MA. 2010. Amyloid plaques disrupt resting state default mode network connectivity in cognitively normal elderly. *Biol Psychiatry*. 67:584-587.
- Sorg C, Riedl V, Muhlau M, Calhoun VD, Eichele T, Laer L, Drzezga A, Forstl H, Kurz A, Zimmer C, et al. 2007. Selective changes of resting-state networks in individuals at risk for Alzheimer's disease. *Proc Natl Acad Sci U S A*. 104:18760-18765.
- Sperling RA, Laviolette PS, O'Keefe K, O'Brien J, Rentz DM, Pihlajamaki M, Marshall G, Hyman BT, Selkoe DJ, Hedden T, et al. 2009. Amyloid deposition is associated with impaired default network function in older persons without dementia. *Neuron*. 63:178-188.
- Storandt M, Mintun MA, Head D, Morris JC. 2009. Cognitive decline and brain volume loss as signatures of cerebral amyloid-beta peptide deposition identified with Pittsburgh compound B: cognitive decline associated with Abeta deposition. *Arch Neurol*. 66:1476-1481.
- Thompson PM, Hayashi KM, Dutton RA, Chiang MC, Leow AD, Sowell ER, De Zubicaray G, Becker JT, Lopez OL, Aizenstein HJ, et al. 2007. Tracking Alzheimer's disease. *Ann N Y Acad Sci*. 1097:183-214.
- Tomlinson BE, Blessed G, Roth M. 1968. Observations on the brains of non-demented old people. *J Neurol Sci*. 7:331-356.
- Walsh DM, Selkoe DJ. 2007. A beta oligomers—a decade of discovery. *J Neurochem*. 101:1172-1184.
- Wechsler D. 1987a. Wechsler adult intelligence scale-revised. San Antonio (TX): The Psychological Corporation.
- Wechsler D. 1987b. Wechsler memory scale-revised. San Antonio (TX): The Psychological Corporation.
- Zec RF. 1986. The stroop color-word test: a paradigm for procedural learning. *Arch Clin Neuropsychol*. 1:274-275.